Efficient Meshing Scheme for Bodies of Revolution — Application to Physical Optics Prediction of Electromagnetic Scattering

Zohreh Asadi and Vahid Mohtashami*

Abstract—In this paper, we present an efficient meshing scheme for physical optics calculation of electromagnetic scattering from bodies of revolution. Piecewise linear approximation is used to represent the generatrix and circular perimeter of the body's cross section. This results in quadrilateral meshes and enables the application of multilevel search algorithms for efficient determination of the illuminated portion of the surface. Besides, the physical optics surface integral is reduced to a closed form expression using the Gordon's method. Simulation results confirm the proper accuracy and efficiency of the presented algorithm.

1. INTRODUCTION

Physical Optics (PO) is the most widely used method for calculating electromagnetic scattering from electrically large objects [1]. It provides a good compromise between the accuracy of the results and computational efficiency of the simulations [2–4]. The method incorporates Geometrical Optics (GO) to determine the induced surface current and then integrates the current over the illuminated portion of the surface to calculate the scattered field. To accurately determine the illuminated region, the surface of object is represented by a number of meshes. The meshes should be small enough to model the fine details of the geometry. However, the computational cost of determining the illuminated region of the surface increases with the number of meshes. As a result, large meshes are desirable subject to two important constraints: accurate representation of geometry and, at the same time, efficient and accurate calculation of the physical optics integral on each mesh. Therefore, accuracy and efficiency of the physical optics method strongly depends on size, shape and mathematical description of the meshes.

There are two general techniques for geometrical modeling of arbitrary surfaces in electromagnetic problems: parametric representation [5, 6] and facet-based representation [7, 8]. In parametric representation, the surface of an object is usually expressed in terms of Non-Uniform Rational B-Spline (NURBS). By using this method, the surface of bodies with complex geometry is represented with high accuracy. Little computer memory is required to store the geometry, and the NURBS representation is also suitable for body shaping optimization techniques. However, ray intersection test with NURBS surfaces involves iterative numerical methods, and hence, is very time consuming. Therefore, the increased accuracy is achieved at the cost of higher computational burden due to complexity of the intersection test [9]. In the facet-based representation, the surface of the object is usually described in terms of triangular planar patches. The curvature of the object surface can be efficiently included by increasing the number of patches. Besides, the physical optics integral over the planar patches can be reduced to a closed form expression with Gordon's method [10]. Moreover, the intersection test of a ray with a planar surface has a simple analytical solution, which results in low complexity compared to the NURBS surfaces. Hence, this kind of representation is usually performed in practice. Reducing the number and computational cost of ray-object intersection tests plays an important role in efficiency

enhancement of PO-based scattering prediction. This point is much more notable when the angular pattern of backscattering cross section has to be obtained. One approach to finding the intersected patch is ray-patch intersection test [11, 12]. The number of intersection tests for each ray is proportional to the number of patches, which results in high computational cost specially for large complex objects with high number of facets. Therefore, it is necessary to use acceleration techniques to improve the efficiency of this process. For instance, in [13] the kd-tree and in [14, 15] space division algorithm are presented to accelerate the ray-patch intersection test. Another approach is to find the intersection point between the ray and the object by substituting the ray equation into the equation of the object surface [16]. Then search algorithms are used to find the patch containing the intersection point. This approach is very efficient if the surface equation is not mathematically very complicated, and the object geometry permits applying efficient multilevel search algorithms [17]. Such conditions are satisfied in the case of bodies of revolution.

The purpose of the current paper is to present a mesh generation algorithm for efficient inclusion of bodies of revolution in physical optics method. Due to the rotational symmetry, non-uniform quadrilateral meshes will be used to efficiently determine the illuminated region and accurately calculate the physical optics integral. The mesh resolution will be obtained by an algorithmic procedure which takes into account the impact of curvature and frequency on the angle-dependent backscattering cross section of the object.

The remainder of the paper is organized in three sections. The formulation of the method is discussed in Section 2. The simulation results are provided in Section 3. Concluding remarks are given in Section 4.

2. FORMULATION

A surface of revolution is created by rotating a curve, called generatrix, about an axis. Consider a surface of revolution with the generatrix given by $z = f(x)$ whose axis lies along the z-axis. The vertex lies at the origin, and the circular edge lies on the plane $z = H$. Assume that this surface is made up of a certain number of facets. To determine the illuminated facets, a multilevel procedure is employed. The intersection points of the incident rays on the surface are first calculated by using the implicit surface equation, then the enclosing facet for each point is determined by search algorithms. Therefore, the efficiency of finding the illuminated region depends directly on how well these two parts are performed.

Each intersection point is obtained by substituting the parametric representation of the incident ray into the implicit surface equation. This yields a one variable algebraic equation whose solution determines the distance between the source location and the intersection point. For conventional bodies of revolution, the solution to this algebraic equation is the smallest positive root of the polynomial [16].
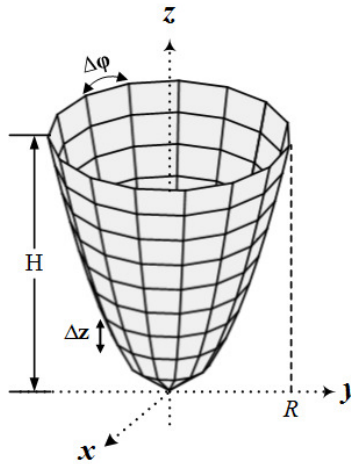

Figure 1. General view of a body of revolution with quadrilateral meshes.

The elliptic, parabolic and secant ogive nose cones are examples of these surfaces. The roots of the polynomial are efficiently obtained analytically or by eigenvalue based methods [18]. More complicated surfaces such as the Von Karman nose cone require iterative numerical methods. After obtaining the intersection point, we have to locate the enclosing patch to calculate its contribution to the scattered field. The computational complexity of search algorithm will be significantly reduced if simple meshing pattern is used. One such pattern is depicted in Figure 1 in which piecewise linear approximation is used in both ϕ and z directions to decompose the surface into quadrilateral patches. By knowing the z and ϕ coordinates of the intersection point, the intersected patch is easily determined. The rotational symmetry guarantees that for a patch in $\phi_1 \leq \phi \leq \phi_2$ and $z_1 \leq z \leq z_2$ the line which passes through the vertices (ϕ_1, z_1) and (ϕ_1, z_2) intersects the z-axis on exactly the same point as the line that passes through the vertices (ϕ_2, z_1) and (ϕ_2, z_2). Therefore, the four vertices of each patch are coplanar and the physical optics surface integral can be efficiently calculated using Gordon's method. The key point is the proper selection of mesh resolution such that the accuracy of the scattered field is not compromised. This is investigated in details in following subsections.

2.1. Approximation in z Direction

Physical optics approximation uses geometrical optics to calculate the induced current density on a surface and then integrating that current over the surface to calculate the scattered field. The scattered magnetic field under these assumptions can be written as [19]

$$\vec{H}^s(r) = \frac{-jk_0}{2\pi r} e^{-jk_0 r} \int_{S_i} e^{jk_0 \vec{r'} \cdot \hat{r}} \hat{r} \times \left(\hat{n}\left(\vec{r'}\right) \times \vec{H}_1\left(\vec{r'}\right) \right) ds' \tag{1}$$

where $\hat{n}\left(\vec{r'}\right)$ is the unit normal vector for a point on the surface located at position vector $\vec{r'}$, k_0 the free space wave number, $\hat{r}$ the unit vector of the direction of observation, $\vec{H}_1 = H_0 e^{-jk_0 \hat{k} \cdot \vec{r'}} \hat{h}_i$ the incident magnetic field, $\hat{k}$ the unit vector of the incident wave direction and S_i the illuminated region on the surface. By using the well-known BAC-CAB rule of vector algebra [1], the far-zone magnetic field can be written as

$$\vec{H}^s(r) = \frac{-jk_0 H_0}{2\pi r} e^{-jk_0 r} \left[\left(\hat{r} \cdot \hat{h}_i\right) \vec{f} - \left(\hat{r} \cdot \vec{f}\right) \hat{h}_i \right] \tag{2}$$

where

$$\vec{f} = \int_{S_i} \hat{n}\left(\vec{r'}\right) exp\left(jk_0(\hat{r} - \hat{k}) \cdot \vec{r'} \right) ds' \tag{3}$$

is called physical optics integral. The problem is to approximate the generatrix of the surface by a piecewise linear function with the minimum number of segments so that the difference between the
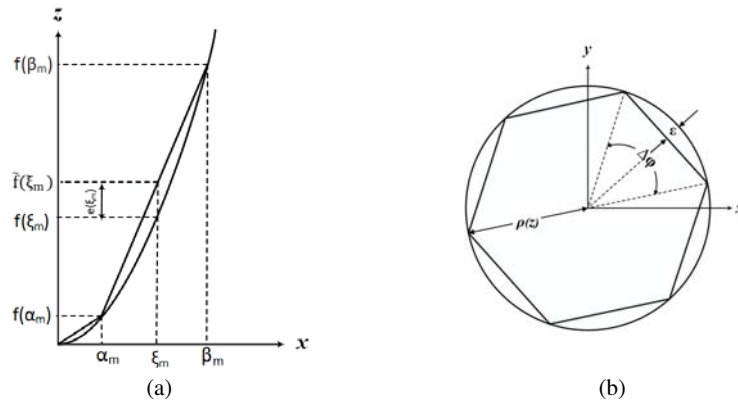

(a)   (b)

Figure 2. Piecewise linear approximation of a surface of revolution (a) in z direction, (b) in ϕ direction.

approximation and the function does not exceed a given error. For the geometry depicted in Figure 2(a), $\widehat{r}, \widehat{k}$, and $\vec{r'}$ are written in Cartesian coordinate as

$$\widehat{r} = \widehat{x}\sin\theta + \widehat{z}cos\theta \tag{4a}$$

$$\widehat{k} = -(\widehat{x}\sin\theta_i + \widehat{z}cos\theta_i) \tag{4b}$$

$$\vec{r'} = \widehat{x}x' + \widehat{z}z' \tag{4c}$$

In high frequency region, the phase of the integrand in physical optics integral varies rapidly in comparison with its amplitude. Hence the phase variation is used as the meshing criteria. Assume that the generatrix function $f(x)$ is approximated by a piecewise linear function $\widetilde{f}(x)$. The phase term of exact and approximated physical optics integral are, respectively

$$\psi(x) = k_0[x(\sin\theta + \sin\theta_i) + f(x)(\cos\theta + \cos\theta_i)] \tag{5a}$$

$$\widetilde{\psi}(x) = k_0[x(\sin\theta + \sin\theta_i) + \widetilde{f}(x)(\cos\theta + \cos\theta_i)] \tag{5b}$$

and the phase difference in mth subinterval, $(\alpha_m \leq x \leq \beta_m)$, is equal to

$$\Delta\psi(x) = k_0[\widetilde{f}(x) - f(x)](\cos\theta_i + \cos\theta) \tag{6}$$

define $e(x) = \widetilde{f}(x) - f(x)$ as the linear interpolation error in this subinterval, as a result $|\Delta\psi(x)| \leq 2k_0|e(x)|$. Given α_m, we wish to find the value of β_m such that the phase error does not exceed ϵ_{max}^z. Due to convexity $\dfrac{d^2f}{dx^2} > 0$, therefore $\dfrac{df}{dx}$ is increasing. Then according to mean value theorem there is a single value $x = \xi_m$ in this subinterval such that $\dfrac{de}{dx} = 0$. At $x = \xi_m$, $|e(x)|$ reaches its maximum which results in maximum phase error. By using straight forward mathematical calculation the equation governing the value of ξ_m is obtained as

$$(\alpha_m - \xi_m)\dfrac{df}{dx}\Big|_{\xi_m} + f(\xi_m) - f(\alpha_m) - \dfrac{\epsilon_{max}^z}{2k_0} = 0 \tag{7}$$

This equation can be solved using analytical or numerical methods depending on the function $f(x)$. Starting from $\alpha_1 = 0$, The value of ξ_1 can be calculated from Eq. (7) for a specified maximum phase error $\Delta\psi_{max} = \epsilon_{max}^z$. As a result, $\widetilde{f}(x)$ is the line that passes through $(\alpha_m, f(\alpha_m))$ and has the slope of $\dfrac{df}{dx}\Big|_{\xi_m}$. The intersection point of $f(x)$ and $\widetilde{f}(x)$ gives β_1. Then set $\alpha_2 = \beta_1$ and repeat the same procedure to find β_2. The process is repeated until the last subinterval exceeds the body's radius. This way the local curvature of the generatrix is effectively taken into account. The smaller local curvature results in larger subinterval which effectively reduces the number of subintervals and facets.

2.2. Approximation in ϕ Direction

In this case, piecewise linear approximation is performed in cross sectional plane. The circular cross section has a constant curvature. Therefore, approximation is performed uniformly by inscribing an N-edge regular polygon in the circle. Due to symmetry, the phase error follows the same trend in each subinterval. As shown in Figure 2(b) this approximation results in a maximum approximation error occurs at the midpoint of each subinterval. By using a similar procedure as the one following Eq. (6), the phase error in each interval is bounded

$$|\Delta\psi(z)| \leq 2k_0\rho(z)\left(1 - \cos\left(\dfrac{\Delta\phi(z)}{2}\right)\right) \tag{8}$$

where $\Delta\phi(z) = \dfrac{2\pi}{N(z)}$ and $\rho(z) = f^{-1}(z)$. The cross section curvature decreases as we move from the nose of the body to the base. Therefore, the number of polygon edges is considered a function of z-coordinate of the circular section. For small values of $\Delta\phi(z)$ we have

$$|\Delta\psi(z)| \leq \dfrac{k_0\pi^2\rho(z)}{N^2(z)} \tag{9}$$

Given a maximum phase error of $\Delta\psi_{\max} = \epsilon_{\max}^{\phi}$, we can find the number of segments in mth subinterval by

$$N(z) = \pi\sqrt{\frac{k_0\bar{\rho}_m}{\epsilon_{\max}^{\phi}}} \tag{10}$$

where $\bar{\rho}_m$ is the average $\rho(z)$ in subinterval $z(\alpha_m) \leq z \leq z(\beta_m)$. Figure 3 shows elliptical and secant ogive nose cones meshed using the proposed method. The curvature near the tip of the elliptical nose cone is higher, which results in finer segments in z-direction. The secant ogive, on the other hand, has constant curvature in z-direction. This results in uniform meshing pattern along the z-axis. In both nose cones, $\bar{\rho}$ increases as we move to the base. According to Eq. (10), the mesh resolution in ϕ direction is an increasing function of z as confirmed by Figure 3.

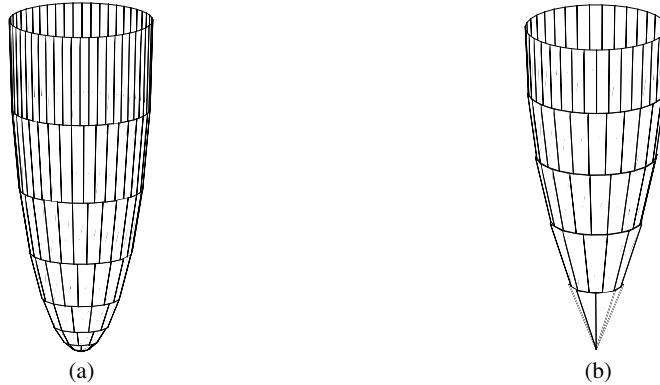(a)   (b)

Figure 3. Mesh generation by presented method for (a) elliptical nose cone, and (b) secant ogive nose cone.

The proposed meshing scheme results in planar quadrilateral patches and hence, the PO integral for each patch can be analytically calculated by Gordon's method [10]. After meshing the surface and determining the illuminated patches, the physical optics integral at an arbitrary illuminated patch, denoted as P_i, can be calculated using the following closed-form representation [10]

$$\vec{f} = \frac{j\hat{n}\left(\vec{r'}\right)}{k_0|\vec{w}|^2}(T_1 + T_2 + T_3 + T_4) \tag{11}$$

where $\vec{w}$ is the projection of $(\hat{r} - \hat{k})$ on P_i plane, and

$$T_n = (\vec{w}^* \cdot \Delta a_n)\frac{\sin[\frac{k_0}{2}\vec{w} \cdot \Delta a_n]}{\frac{k_0}{2}\vec{w} \cdot \Delta a_n} \exp\left[\frac{jk_0}{2}\vec{w} \cdot (\vec{a_n} + \vec{a_{n+1}})\right]; 1 \leq n \leq 4 \tag{12}$$

In this equation, for the vector $\vec{w} = [w_1, w_2]$ in the plane of P_i, $\vec{w}^* = [w_2, -w_1]$ is the vector obtained by rotating $\vec{w}$ at 90° clockwise. The position vectors of vertices of quadrilateral mesh in P_i plane are denoted as $\vec{a_1}, \vec{a_2}, \vec{a_3}, \vec{a_4}$. The value of $\vec{a_5}$ is taken the same as $\vec{a_1}$ and $\Delta a_n = \vec{a_{n+1}} - \vec{a_n}$.

3. SIMULATION RESULTS AND DISCUSSION

The developed simulation code in this research calculates the PO integral in both monostatic and bistatic scenarios by using the Gordon's method [10]. Multiple reflections that occur in complex geometries are included via the well-known multiple GO + PO approach [20]. The code includes the effect of surface curvature on the electromagnetic field amplitude in multiple reflections [21, 22] and calculates the diffraction and reflection-diffraction fields via the Method of Equivalent Currents [23]. In order to verify the proposed meshing algorithm, scattering from two typical benchmark objects are studied and
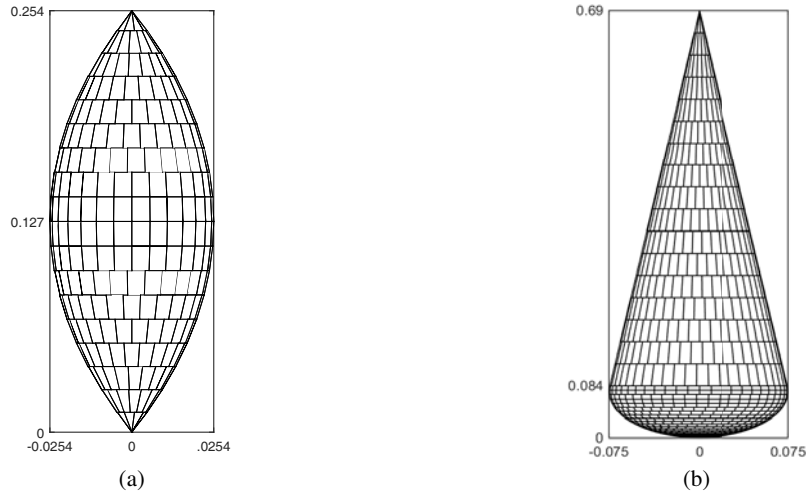
Figure 4. Mesh generation by presented method for a (a) single ogive, and (b) cone-sphere.

compared with experimental data and numerical methods. The first example is an ogive as depicted in Figure 4(a). The ogive has a half length of 0.127 m and a maximum radius of 0.0254 m. For meshing the surface, the maximum phase errors in z and ϕ direction are set to $\pi/200$ and $\pi/100$, respectively. The linear approximation in z direction leads to 28 segments. Then the number of segments in ϕ direction is obtained for each subinterval according to (10). As a result, the surface is modeled with 786 non-uniform quadrilateral patches. The backscattering cross section is computed in $\phi = 0$ plane for incident angles $0°$ to $180°$ with angular resolution of $0.5°$ at 9 GHz. The incident angles $\theta = 0, 180°$ correspond to axial incidence. The procedure is repeated for a medium mesh resolution with $\epsilon_{max}^z = \pi/100$ and $\epsilon_{max}^{\phi} = \pi/50$, which results in 396 patches. The backscattering cross section for both high and medium mesh resolutions is obtained and compared with measurement data [24] in Figure 5(a). VV polarization is assumed but similar results are obtained for HH polarization. The PO simulation results from the commercial *FEKO* software [25] is also included in this figure. As observed, the scattering results from proposed method with high mesh resolution can yield the same accuracy as the physical optics simulation in *FEKO*. The discrepancies between the simulations and the measurements, specially for angles near axial incidence are attributed to the errors caused by the faceting of the curved surface and ignoring the creeping waves and tip diffraction effects. When using measurements as the reference values, one must take special care because measurement data may not be very accurate. This is due to a variety of sources such as measuring instruments or human factors. However, the geometries that are meshed and simulated in this paper are benchmark targets that are provided for the validation of computational electromagnetics programs by the Electromagnetic Code Consortium (EMCC) [24]. Furthermore, our simulation results are compared with physical optics results of *FEKO* which demonstrate the proper accuracy of the presented method. In Figure 5(b) the bistatic radar cross section for high mesh resolution is computed by our code in $\phi = 90°$ plane for incident angle $\theta_i = 45°$ and observation angles $0°$ to $180°$ at 9 GHz. The result is compared with the physical optics simulation of *FEKO* as well as Multi-Level Fast Multipole Method (MLFMM) as an accurate numerical method. As observed, our simulation results agree well with the physical optics simulation in *FEKO*. Our results exhibit the same level of error as the physical optics simulation of *FEKO* with respect to MLFMM.

The second example is a cone-sphere with a half angle of 7 degrees and a radius of 0.075 m. The length of object is 0.69 m, and the side of the cone is tangent to the sphere, which results in negligible diffraction at the joint. The surface is meshed using high and medium mesh resolution, leading to 2478 and 1409 patches, respectively. The meshed surface is depicted in Figure 4(b). The backscattering cross section for both medium and high mesh resolutions are computed in $\phi = 0$ plane for incident angles $0°$ to $180°$ with angular resolution of $0.5°$ at 9 GHz. The results are compared with measurement data for VV polarization [24] and physical optics simulation of *FEKO* in Figure 6(a). As observed, the results
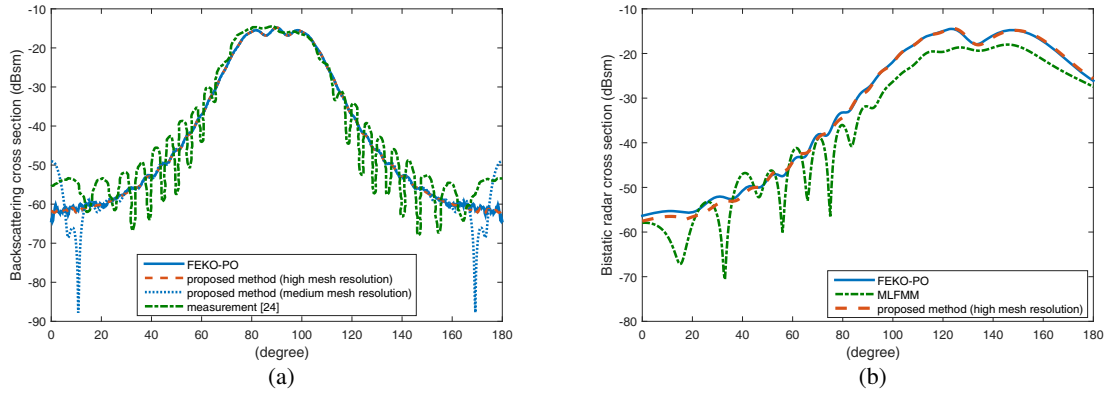
Figure 5. Monostatic and bistatic radar cross section pattern for single ogive (a) monostatic, (b) bistatic ($\theta_i = 45°$).
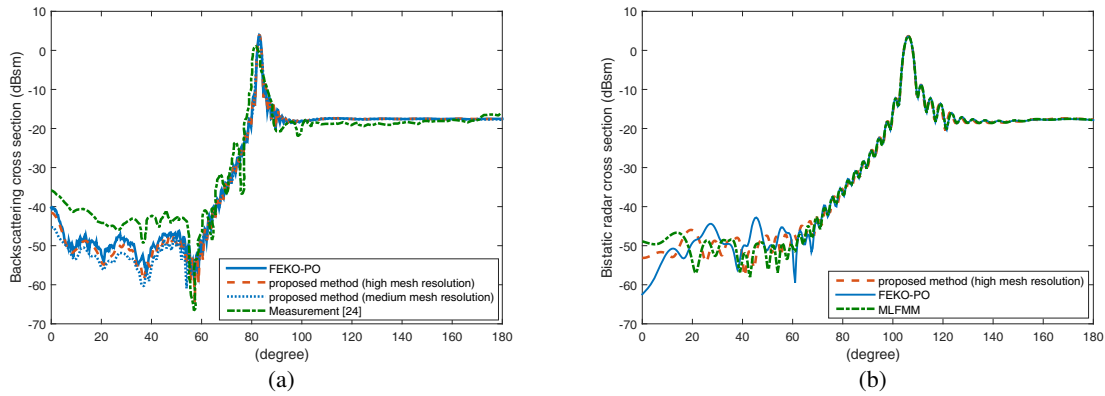

Figure 6. Monostatic and bistatic radar cross section pattern for cone-sphere (a) monostatic, (b) bistatic ($\theta_i = 60°$).

of our proposed method yields the same accuracy as *FEKO*. The differences between simulation results and measured data are due to neglecting the tip and surface diffracted rays. The bistatic radar cross section for high mesh resolution is also computed at 9 GHz in $\phi = 90°$ plane for incident angle $\theta_i = 60°$ and observation angles 0° to 180°. The result is compared with those of physical optics simulation of *FEKO* and MLFMM in Figure 6(b). The results obtained from our code with the proposed meshing scheme has good agreement with those obtained from physical optics simulation of *FEKO* as well as MLFMM.

To achieve backscattering cross section with desired level of accuracy, the mesh resolutions in z and ϕ directions have to be adjusted. Decreasing $\epsilon_{\max}^z$ and $\epsilon_{\max}^\phi$ increases the accuracy of backscattering cross section calculation at the cost of increasing the processing time. The meshing procedure is done for various bodies of revolution to calibrate $\epsilon_{\max}^z$ and $\epsilon_{\max}^\phi$. In each case, the absolute value of the error between the result of our proposed method and the exact solution is computed in dB at all incidence angles. The mean error and 95% confidence interval is obtained accordingly for the considered values of $\epsilon_{\max}^z$ and $\epsilon_{\max}^\phi$.

The exact solution is obtained by numerical calculation of physical optics integral using global adaptive quadrature [26]. In error calculation, the samples less than 40 dB below the maximum value are neglected. The proposed meshing procedure is performed for various types of nose cone shapes involving parabolic, elliptical, secant ogive, tangent ogive and power series. Different values of $\epsilon_{\max}^z$ and $\epsilon_{\max}^\phi$ are obtained for different nose cones. However, in order to provide a general rule of thumb, the

Table 1. Values of maximum phase error in ϕ and z directions and the corresponding error of backscattering cross section results.

Mean error (dB)	Confidence Interval (dB)	$\epsilon_{\max}^{\phi}$	$\epsilon_{\max}^{z}$
1	[0.7, 1.2]	$\pi/32$	$\pi/20$
0.5	[0.3, 0.7]	$\pi/50$	$\pi/40$

Table 2. Total number of patches and computation time of different methods in ellipsoid backscattering cross section prediction.

Method	No. of patches	Meshing time (s)	Computation time (s)
Proposed method	720	0.65	22
Delaunay triangulation	1308	1.5	97
FEKO-PO	9422	3	48

upper bounds for $\epsilon_{\max}^{z}$ and $\epsilon_{\max}^{\phi}$ are reported in Table 1 for the desired level of accuracy. The values provided in this table applies to meshing all considered bodies of revolution irrespective of their physical dimensions and the frequency.

According to Eqs. (6) and (8), the criteria for mesh resolution is determined based on the incident wavelength (frequency). In some cases, the length of meshes are more than three times the wavelength. For example, in Figure 3, the generatrix of secant ogive nose cone is divided into 5 equal segments. The height of nose cone is 0.54 m and the frequency is 9 GHz, so the length of meshes are 3.24 times the wavelength in z direction. This is a desirable property which reduces the computational time throughout the main PO simulation. Note that a geometrical criteria can also be used to ensure that the meshing scheme is applicable in low frequencies as well. For instance, the mesh resolution in ϕ direction can be chosen in a way that the area of the inscribed polygon exceeds 90% of area of the circular section. In z direction, the longest segment can be set to be shorter than the half of the smallest dimension of object. By applying such extended criteria, the proposed algorithm can also be used for bodies of revolution with zero Gaussian curvature such as cone and cylinder. Such geometrical criteria can also be used to generate quadrilateral meshes on planar surfaces such as dihedral and trihedral corner reflectors.

To evaluate the computational efficiency of proposed method, the surface of an ellipsoid is meshed by the presented method as well as by the Delaunay triangulation [27]. The object has a half-length of 0.54 m and a base radius of 0.09 m. The values of $\epsilon_{\max}^{\phi}$ and $\epsilon_{\max}^{z}$ in proposed method are set to $\pi/32$ and $\pi/20$, respectively. As a result, the surface is modeled with 720 quadrilateral patches. To determine the illuminated patches in the quadrilateral mesh, the simple multilevel procedure described in Section 2 is used. Then the backscattering cross section is computed in $\phi = 0$ plane for incident angles $0° \leq \theta \leq 180°$ with angular resolution of $1°$ at 9 GHz. The results are compared with physical optics simulation of *FEKO* within 0.7 dB mean difference. In order to make a fair comparison, the mesh resolution in Delaunay triangulation method is chosen such that the result has the similar level of accuracy with respect to *FEKO* simulation. In both methods, scattering field contribution of each illuminated patch is calculated using Gordon's method. In Table 2 the total number of patches and runtime performances of these methods are reported. By using the quadrilateral patches, runtime speedup of about $97/22 = 4.4$ times is obtained compared to Delaunay triangulation. In the proposed method, the mesh generation procedure is performed very quickly and the number of patches is much less than those of other techniques. Note that the ray-object intersection tests in our simulations are done without conventional acceleration techniques whereas commercial *FEKO* software uses various acceleration algorithms in ray tracing and PO integral calculation. The efficiency of our simulation is due to the proposed meshing scheme that simplifies that determination of the illuminated portion of the object without compromising the accuracy. It should be noted that *FEKO* is a comprehensive computational electromagnetic software for the electromagnetic field analysis of arbitrarily shaped

structures. By presenting the entries of Table 2 we do not intend to show the superiority of our code to the FEKO; rather, we want to emphasize that the proposed meshing scheme improves the computational performance of PO calculations for bodies of revolution. The presented meshing scheme is therefore suggested to be implemented in a commercial software that includes this kind of geometry.

4. CONCLUSION

In this paper, we introduce a mesh generation scheme for efficient calculation of electromagnetic scattering from electrically large bodies of revolution. The curvature of the surface is approximated by piecewise linear function in both directions, thereby meshing the surfaces into quadrilateral patches. This enables finding the illuminated part of the surface through an efficient multilevel intersection test. Furthermore, each four points defining a quadrilateral patch are coplanar. This results in closed-form and hence efficient computation of physical optics integral.

The mesh resolution is adjusted according to the curvature of the object, frequency and the desired level of accuracy. The procedure is based on deriving suitable upper bounds for phase error of the physical optics integral. The upper bounds have been adjusted for various nose cones and thereby a guideline is provided for meshing the surface. The simulation results show that the size of quadrilateral meshes can be as large as several wavelengths with less than 1 dB error in backscattering cross section calculation. As a result, the number of meshes and consequently the simulation time can be efficiently reduced.

REFERENCES

1. Balanis, C. A., *Advanced Engineering Electromagnetics*, Wiley, 1989.
2. Uluisik, C., G. Cakir, M. Cakir, and L. Sevgi, "Radar cross section (RCS) modeling and simulation, Part 1: A tutorial review of definitions, strategies, and canonical examples," *IEEE Antennas and Propagation Magazine*, Vol. 50, No. 1, 115–126, Feb. 2008.
3. Fan, T., L. Guo, B. Lv, and W. Liu, "An improved backward SBR-PO/PTD hybrid method for the backward scattering prediction of an electrically large target," *IEEE Antennas and Wireless Propagation Letters*, Vol. 15, 512–515, 2015.
4. Hemon, R., P. Pouliguen, H. He, J. Saillard, and J.-F. Damiens, "Computation of EM field scattered by an open-ended cavity and by a cavity under radome using the iterative physical optics," *Progress In Electromagnetics Research*, Vol. 80, 77–105, 2008.
5. Della Giovampaola, C., G. Carluccio, F. Puggelli, A. Toccafondi, and M. Albani, "Efficient algorithm for the evaluation of the physical optics scattering by NURBS surfaces with relatively general boundary condition," *IEEE Transactions on Antennas and Propagation*, Vol. 61, No. 8, 4194–4203, Aug. 2013.
6. Zhao, Y., X.-W. Shi, and L. Xu, "Modeling with NURBS surfaces used for the calculation of RCS," *Progress In Electromagnetics Research*, Vol. 78, 49–59, 2008.
7. Youssef, N., "Radar cross section of complex targets," *Proceedings of the IEEE*, Vol. 77, No. 5, 722–734, May 1989.
8. Weinmann, F., "Ray tracing with PO/PTD for RCS modeling of large complex objects," *IEEE Transactions on Antennas and Propagation*, Vol. 54, No. 6, 1797–1806, Jun. 2006.
9. Domingo, M., F. Rivas, J. Perez, R. Torres, and M. F. Catedra, "Computation of the RCS of complex bodies modeled using NURBS surfaces," *IEEE Antennas and Propagation Magazine*, Vol. 37, No. 6, 36–47, Dec. 1995.
10. Gordon, W., "Far-field approximations to the Kirchoff-Helmholtz representations of scattered fields," *IEEE Transactions on Antennas and Propagation*, Vol. 23, No. 4, 590–592, Jul. 1975.
11. Havel, J. and A. Herout, "Yet faster ray-triangle intersection (using SSE4)," *IEEE Transactions on Visualization and Computer Graphics*, Vol. 16, No. 3, 434–438, May 2010.
12. Woop, S., C. Benthin, and I. Wald, "Watertight ray/triangle intersection," *Journal of Computer Graphics Techniques*, Vol. 2, No. 1, 65–82, 2013.

13. Tao, Y.-B., H. Lin, and H.-J. Bao, "Kd-tree based fast ray tracing for RCS prediction," *Progress In Electromagnetics Research*, Vol. 81, 329–341, 2008.

14. Jin, K.-S., T.-I. Suh, S.-H. Suk, B.-C. Kim, and H. T. Kim, "Fast ray tracing using a space-division algorithm for RCS prediction," *Journal of Electromagnetic Waves and Applications*, Vol. 20, No. 1, 119–126, 2006.

15. Bang, J.-K., B.-C. Kim, S.-H. Suk, K.-S. Jin, and H.-T. Kim, "Time consumption reduction of ray tracing for RCS prediction using efficient grid division and space division algorithms," *Journal of Electromagnetic Waves and Applications*, Vol. 21, No. 6, 829–840, 2007.

16. Glassner, S., *An Introduction to Ray Tracing*, Academic Press, 1989.

17. Knoll, A., Y. Hijazi, A. Kensler, M. Schott, C. Hansen, and H. Hagen, "Fast ray tracing of arbitrary implicit surfaces with interval and affine arithmetic," *Journal of Computer Graphics Forum*, Vol. 28, No. 1, 26–40, 2009.

18. Saad, Y., *Numerical Methods for Large Eigenvalue Problems*, 2nd Edition, SIAM, Philadelphia, 2011.

19. Knott, E. F., J. F. Shaeffer, and M. T. Tuley, *Radar Cross Section*, 2nd Edition, Artech House, Boston, MA, 1993.

20. Griesser, T. and C. Balanis, "Backscatter analysis of dihedral corner reflectors using physical optics and the physical theory of diffraction," *IEEE Transactions on Antennas and Propagation*, Vol. 35, No. 10, 1137–1147, Oct. 1987.

21. Weinmann, F., "Curvature interpolation of facetted surfaces for high-frequency RCS simulations," *2008 IEEE Antennas and Propagation Society International Symposium*, 1–4, Jul. 2008.

22. Huang, W. F., Z. Zhao, R. Zhao, J. Y. Wang, Z. Nie, and Q. H. Liu, "GO/PO and PTD with virtual divergence factor for fast analysis of scattering from concave complex targets," *IEEE Transactions on Antennas and Propagation*, Vol. 63, No. 5, 2170–2179, May 2015.

23. Michaeli, A., "Equivalent edge currents for arbitrary aspects of observation," *IEEE Transactions on Antennas and Propagation*, Vol. 32, No. 3, 252–258, Mar. 1984.

24. Woo, A., H. Wang, M. Schuh, and M. Sanders, "EM programmer's notebook-benchmark radar targets for the validation of computational electromagnetics programs," *IEEE Antennas and Propagation Magazine*, Vol. 35, No. 1, 84–89, Feb. 1993.

25. [Online]. Available: https://www.feko.info/.

26. Shampine, L., "Vectorized adaptive quadrature in MATLAB," *Journal of Computational and Applied Mathematics*, Vol. 211, No. 11, 131–140, Feb. 2008.

27. Persson, P.-O. and G. Strang, "A simple mesh generator in MATLAB," *SIAM Review*, Vol. 46, No. 2, 329–345, Jun. 2004.